Electronic Supplementary Material (ESI) for Journal of Materials Chemistry C.

Supplementary Information

Active refractive index control using a stably evaporable perfluororesin for high-outcoupling-efficiency organic light-emitting diodes

Daisuke Yokoyama, Tatsuki Sasaki, Yasutaka Suzuki, Takefumi Abe, Kaori Tsuruoka, Tatsuya Miyajima, Toshifumi Kakiuchi, Chiho Morita, Masaharu Aoki, Yasuhiro Ouchi, Wataru Aita, Yasuhiro Kuwana, Yutaka Noguchi*

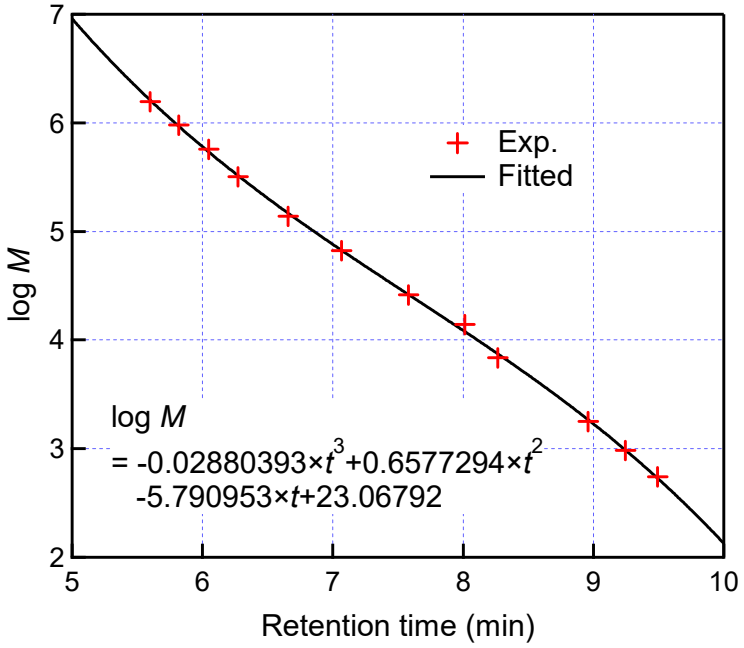

Fig. S1 Calibration curve of SEC determined using solutions of standard samples of polymethyl methacrylate with known molecular weights of the peak maxima.

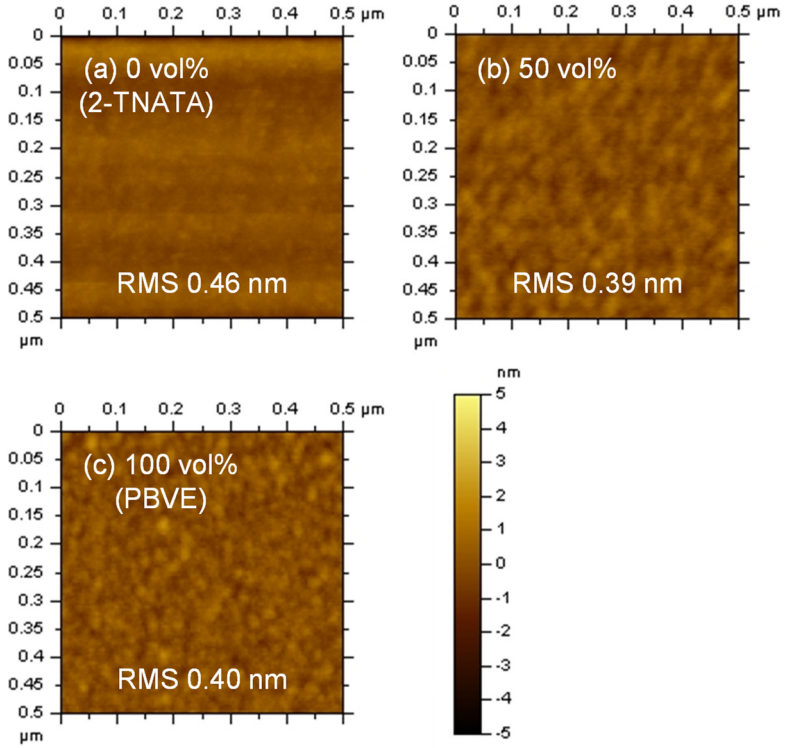

Fig. S2 AFM images of the surfaces of 10-nm-thick neat and co-deposited 2-TNATA:PBVE films with 0, 50, and 100 vol% PBVE on a Si(100) substrate.

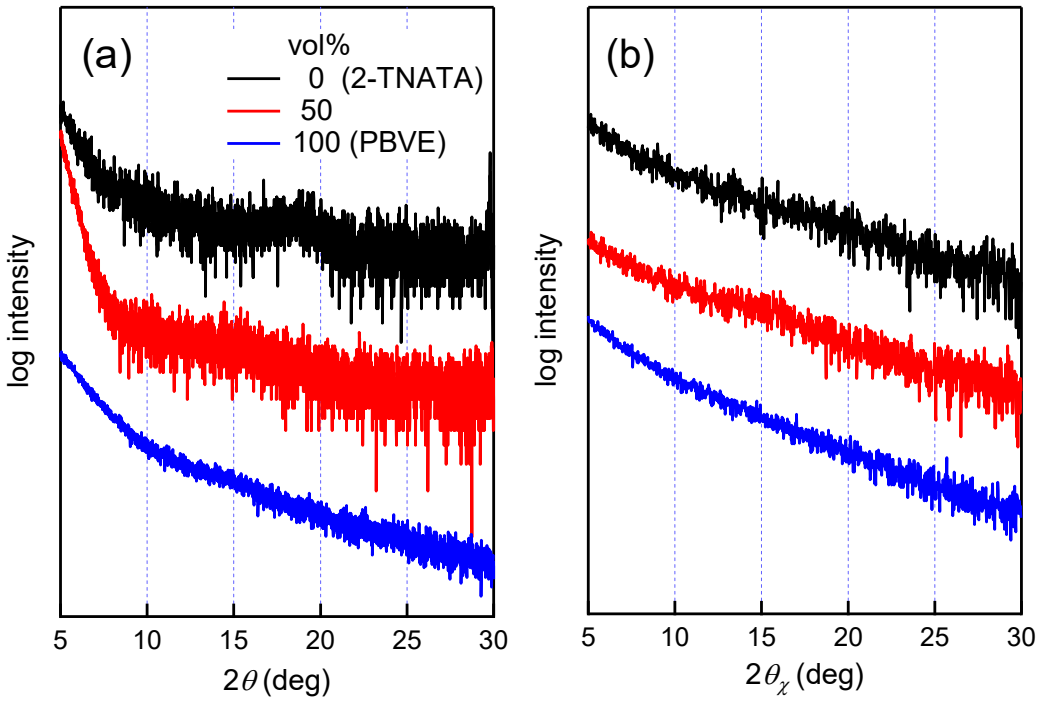

Fig. S3 (a) Out-of-plane and (b) in-plane XRD patterns of 100-nm-thick neat and co-deposited 2-TNATA:PBVE films with 0, 50, and 100 vol% PBVE on a Si(100) substrate.

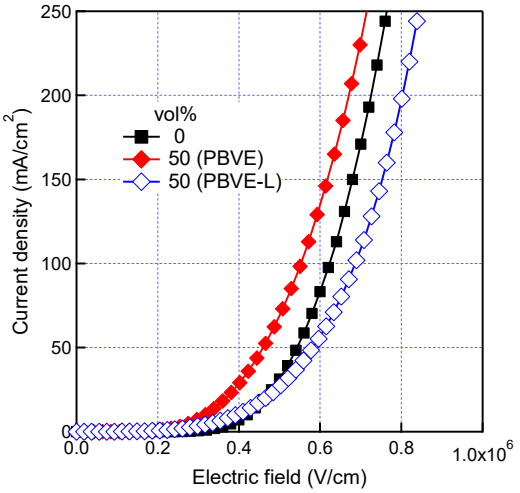

Fig. S4 *J-E* characteristics of hole-only devices of ITO/2-TNATA:PBVE-L (100 nm)/Al (100 nm) with 50 vol% PBVE-L. For comparison, *J-E* characteristics of hole-only devices of ITO/2-TNATA:PBVE (100 nm)/Al (100 nm) with 0 and 50 vol% PBVE are also shown.

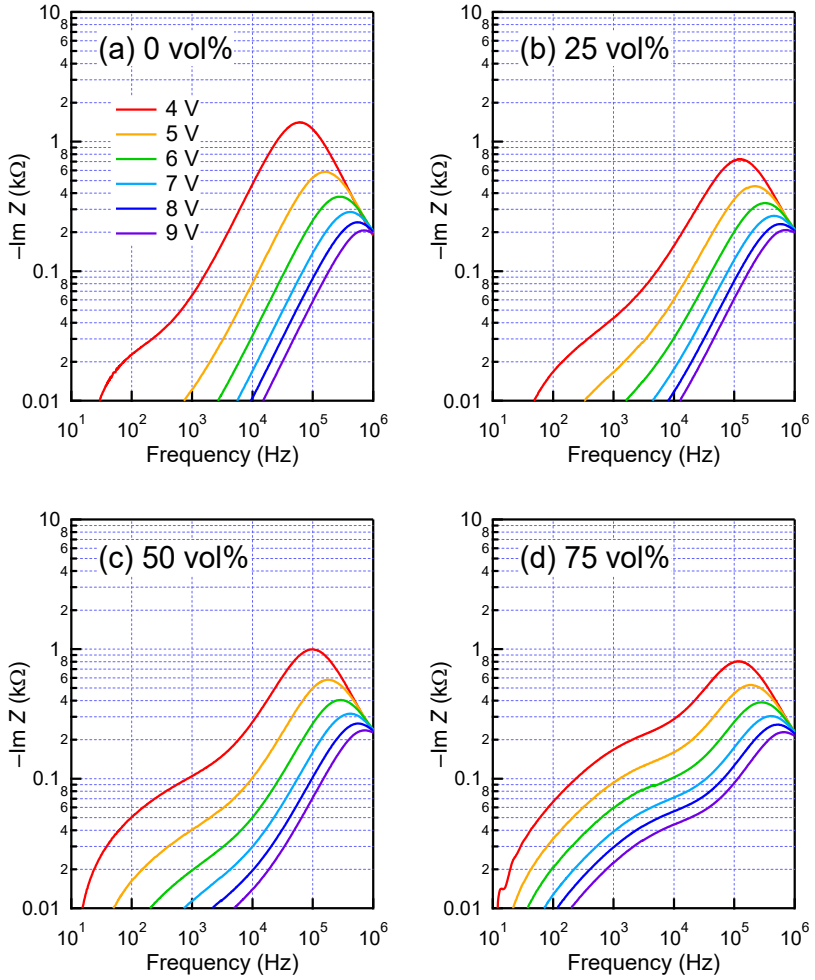

Fig. S5 Imaginary part of the impedance of hole-only devices of ITO/2-TNATA:PBVE (100 nm)/Al (100 nm) with (a) 0, (b) 25, (c) 50, and (d) 75 vol% PBVE under various DC bias voltages.

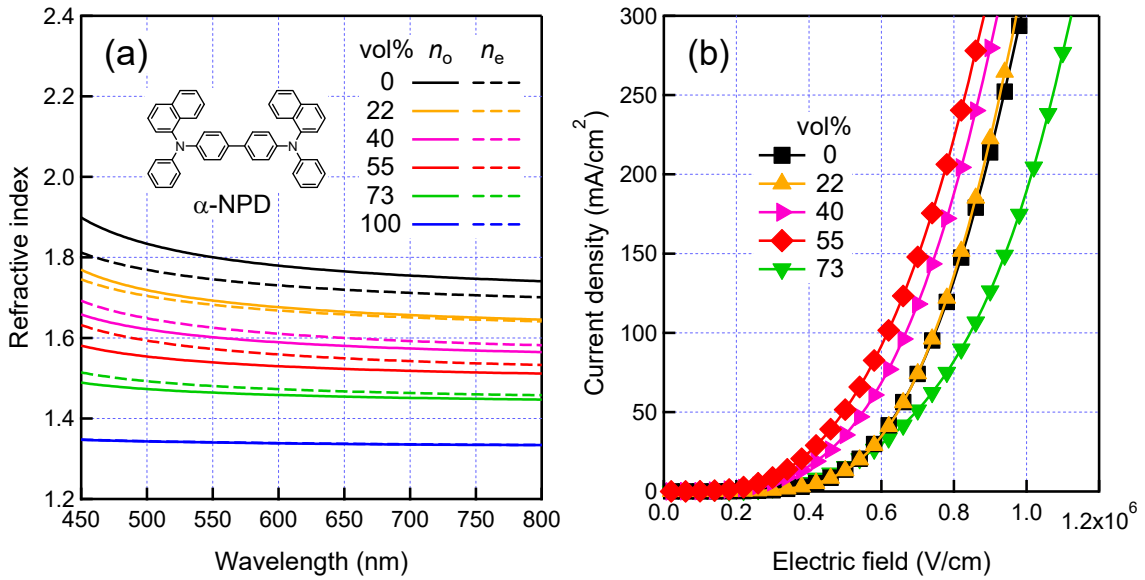

Fig. S6 (a) Ordinary and extraordinary refractive indices of neat and co-deposited α-NPD:PBVE films with 0, 22, 40, 55, 73, and 100 vol% PBVE. (b) *J-E* characteristics of hole-only devices of ITO/MoO_3 (5 nm)/α-NPD:PBVE (100 nm)/MoO_3 (10 nm)/Al (100 nm) with 0, 22, 40, 55, and 73 vol% PBVE.

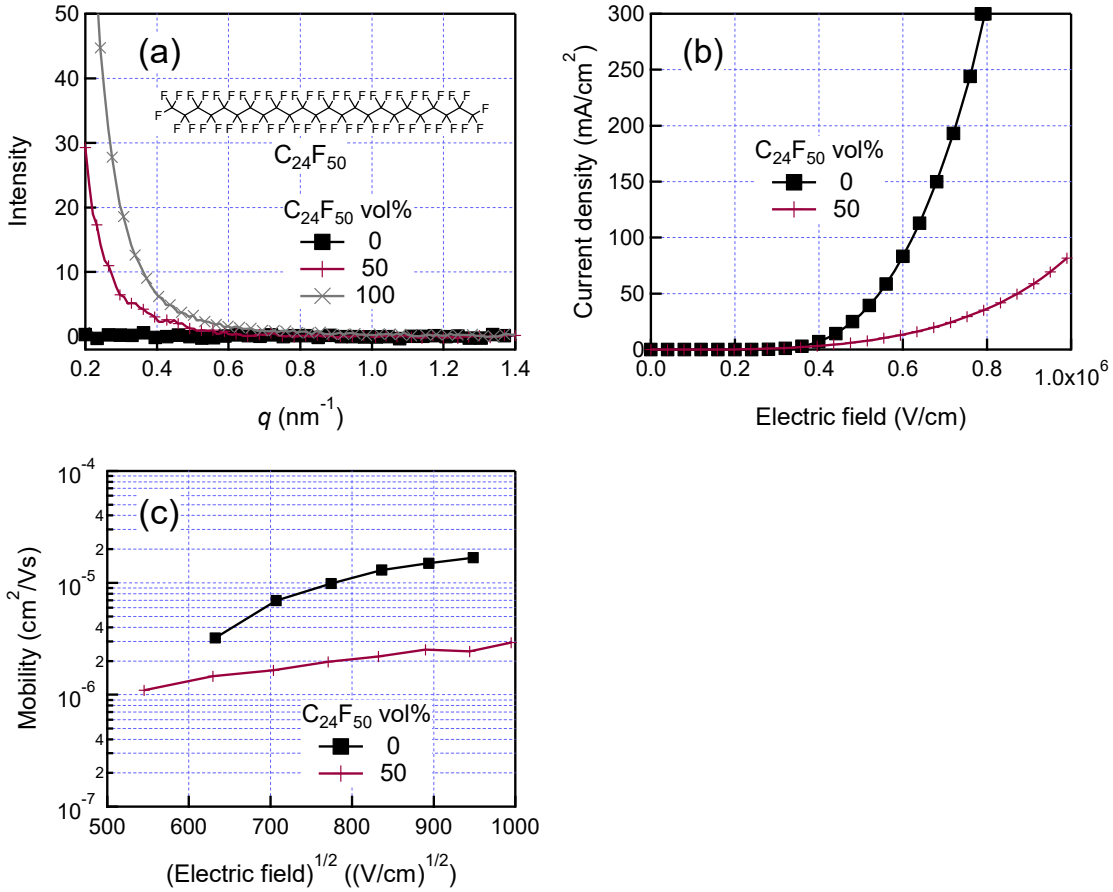

Fig. S7 (a) SAXS profiles of 100-nm-thick neat and co-deposited 2-TNATA:$C_{24}F_{50}$ films with 0, 50, and 100 vol% $C_{24}F_{50}$ on a COP substrate. (b) *J-E* characteristics and (c) hole mobilities measured using hole-only devices of ITO/2-TNATA:$C_{24}F_{50}$ (100 nm)/Al (100 nm) with 0 and 50 vol% $C_{24}F_{50}$.

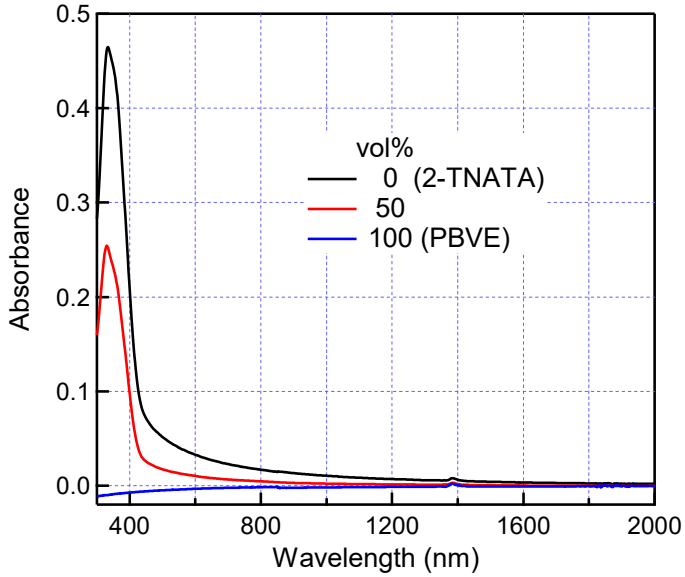

Fig. S8 (a) Visible/NIR absorption spectra of 50-nm-thick neat and co-deposited 2-TNATA:PBVE films with 0, 50, and 100 vol% PBVE on a fused silica substrate.

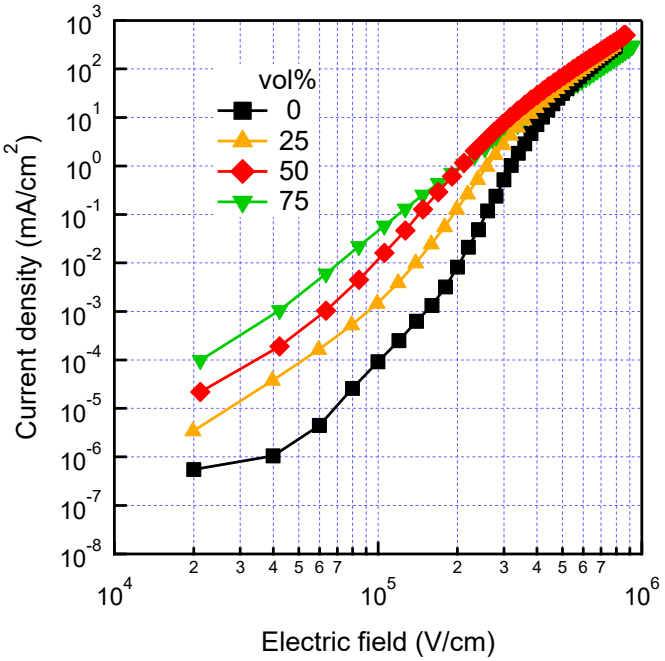

Fig. S9 *J-E* characteristics shown in double logarithmic plot of hole-only devices of ITO/2-TNATA:PBVE (100 nm)/Al (100 nm) with 0, 25, 50, and 75 vol% PBVE (the same data as those in Figure 3(a) shown in linear plot).

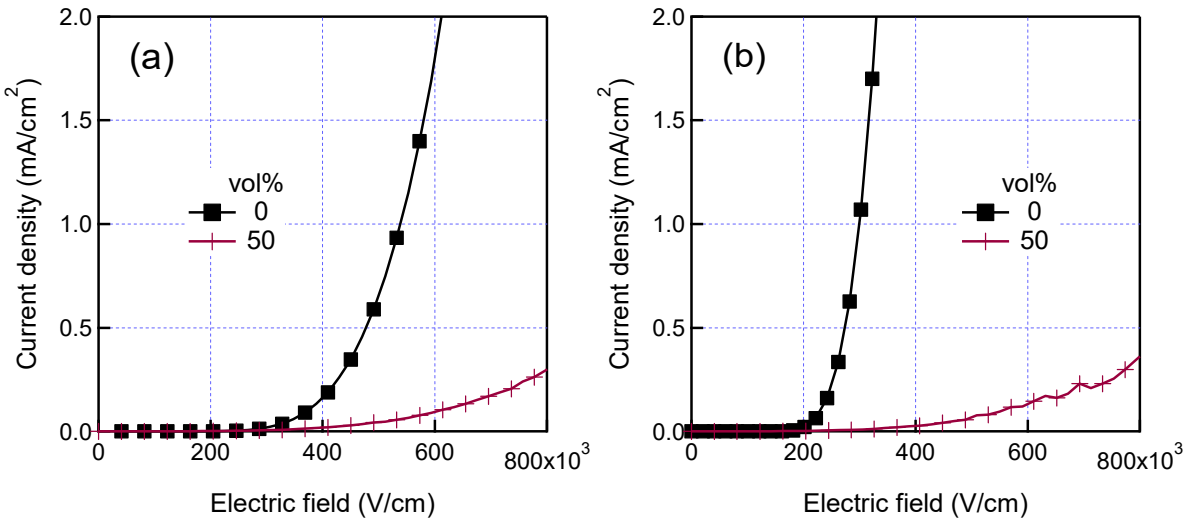

Fig. S10 *J-E* characteristics of electron-only devices of (a) ITO/$CsCO_3$ (1 nm)/Alq_3:PBVE (100 nm)/LiF (1 nm)/Al (100 nm) and (b) ITO/$CsCO_3$ (1 nm)/TPBi:PBVE (100 nm)/LiF (1 nm)/Al (100 nm) with 0 and 50 vol% PBVE, where Alq_3 is tris-(8-hydroxyquinolate)aluminum.

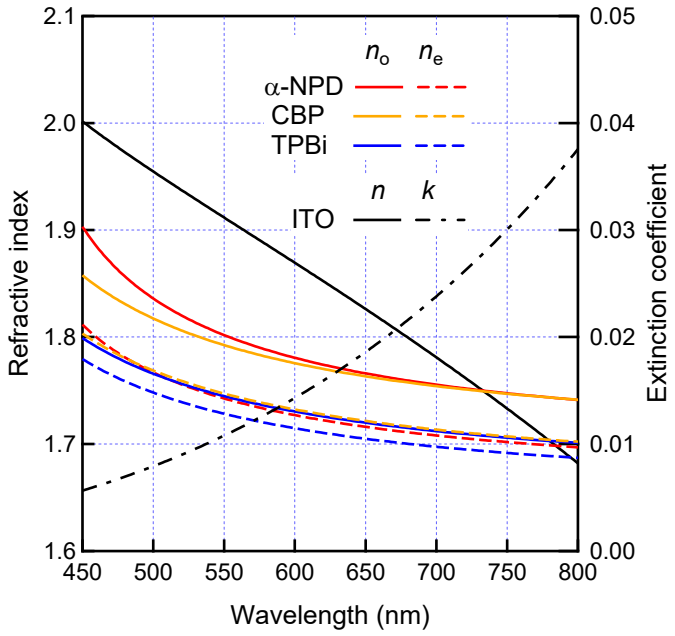

Fig. S11 Ordinary and extraordinary refractive indices of α-NPD, CBP, and TPBi layers and isotropic refractive index and extinction coefficient of the ITO layer used for devices.

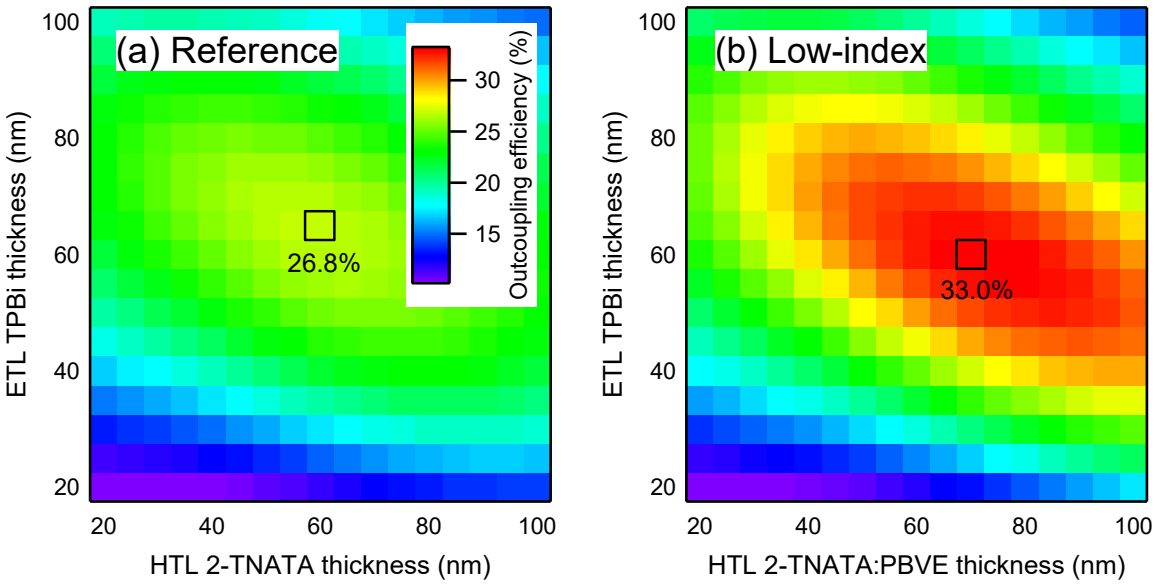

Fig. S12 Dependence of the outcoupling efficiencies of the reference and low-index devices on HTL and ETL thicknesses. Small squares indicate pairs of thicknesses at which the outcoupling efficiencies are maximized.

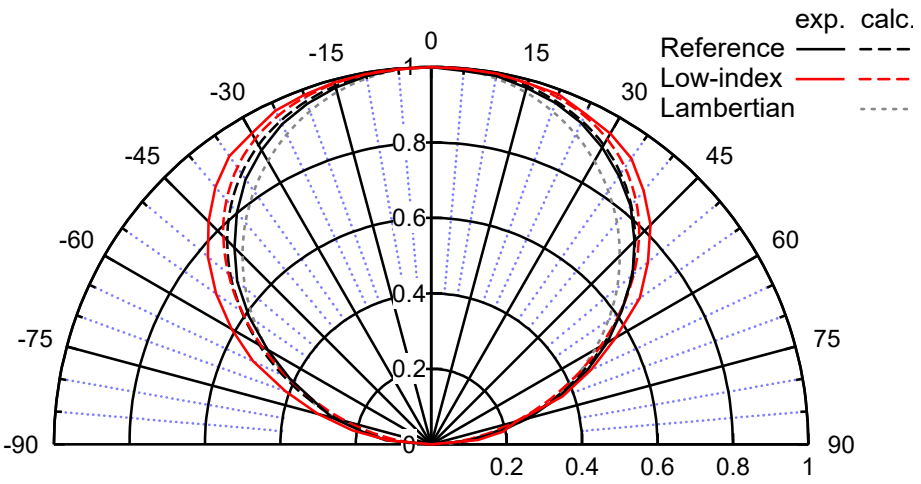

Fig. S13 Angular distributions of the electroluminescence of the reference and low-index devices. Along with the experimental distributions, the simulated and Lambertian distributions are also shown.

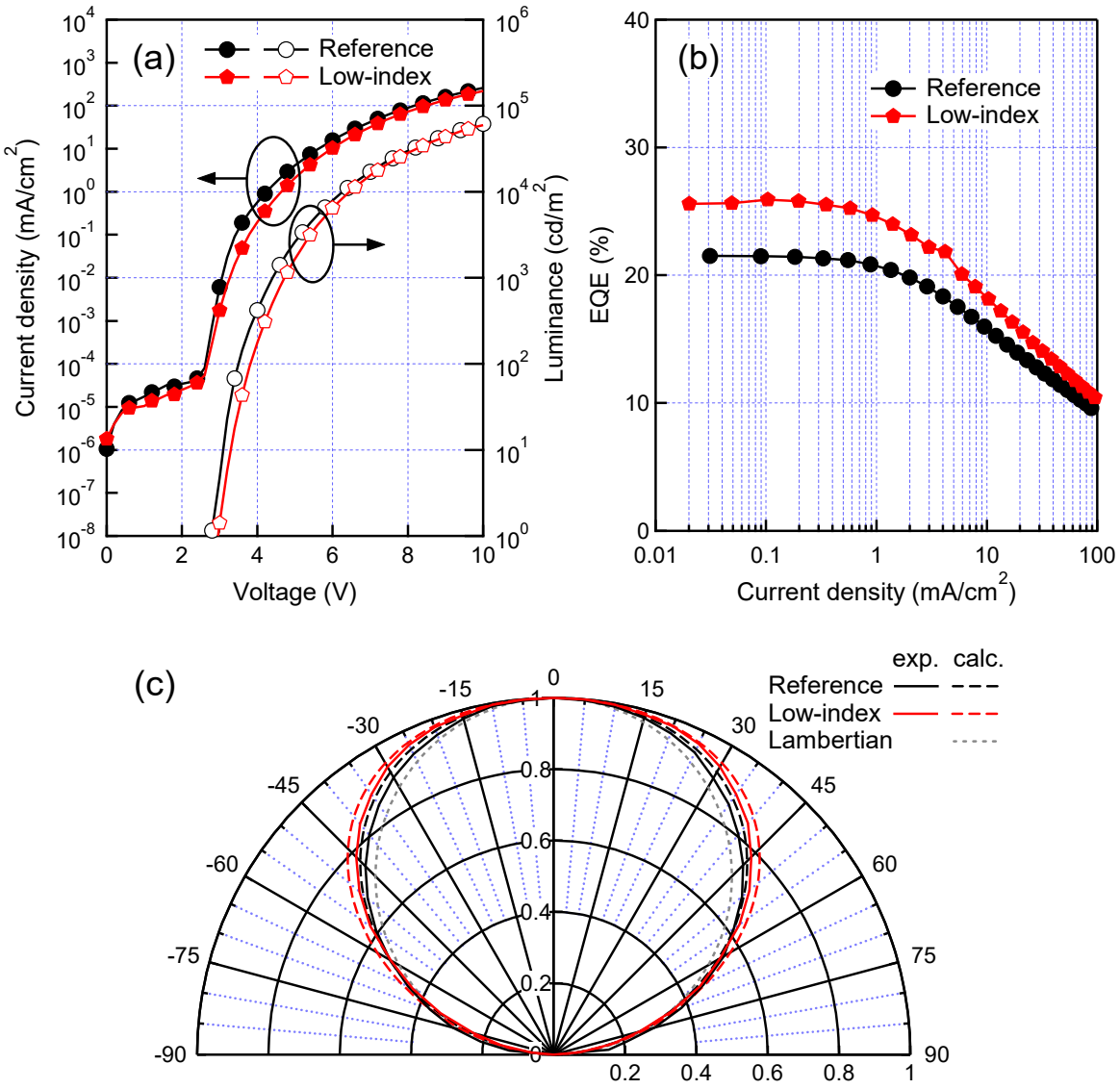

Fig. S14 (a) *J-V-L* characteristics, (b) EQEs, and (c) angular distributions of the electroluminescence of reference and low-index devices that used an α-NPD and α-NPD:PBVE layer as the HTL, respectively. The structures of the reference and low-index devices were glass/ITO (100 nm)/MoO_3 (5 nm)/α-NPD (45 nm)/CBP:Ir(ppy)$_2$(acac) (8 wt%, 15 nm)/TPBi (65 nm)/LiF (1 nm)/Al (100 nm) and glass/ITO (100 nm)/MoO_3 (5 nm)/α-NPD:PBVE (55 vol%, 60 nm)/α-NPD (10 nm)/CBP:Ir(ppy)$_2$(acac) (8 wt%, 15 nm)/TPBi (60 nm)/LiF (1 nm)/Al (100 nm), respectively, where the HTL and ETL thicknesses were optimized using optical simulations so that the outcoupling efficiencies were maximized.